



Sulfate radical-mediated degradation and mineralization of bisphenol F in neutral medium by the novel magnetic $\text{Sr}_2\text{CoFeO}_6$ double perovskite oxide catalyzed peroxymonosulfate: Influence of co-existing chemicals and UV irradiation

Samia Ben Hammouda^{a,*}, Feiping Zhao^a, Zahra Safaei^a, Deepika Lakshamy Ramasamy^{a,b}, Bhairavi Doshi^{a,b}, Mika Sillanpää^{a,b,*}

^a Laboratory of Green Chemistry, School of Engineering Science, Lappeenranta University of Technology, Sammonkatu 12, FI-50130 Mikkeli, Finland

^b Department of Civil and Environmental Engineering, Florida International University, Miami, FL 33174, USA

ARTICLE INFO

Keywords:

Perovskite
Bisphenol F
Sulfate radicals
Mediated degradation

ABSTRACT

Metal-based catalysis has notably contributed to the chemical community mainly in environmental science. Various cobalt and iron based catalysts have shown great potential for powerful reactive species. However, the application of cobalt and iron based perovskite for aqueous phase oxidation still remains limited. In this study, $\text{Sr}_2\text{FeCoO}_6$ double perovskite oxide was synthesized and used for the first time as an effective heterogeneous magnetic catalyst for peroxymonosulfate activation to produce free reactive radicals. Bisphenol F (BPF), a new emergent compound, was used as a target contaminant to evaluate the performance of this combination.

$\text{Sr}_2\text{FeCoO}_6$ exhibited superior catalytic performance to the single SrFeO_3 and SrCoO_3 nanocrystals. A synergetic catalytic effect was found between Co and Fe, probably due to the accelerated reduction of Fe. BPF removal depends on catalyst loading, temperature, BPF and PMS concentration. It was observed that $\text{Sr}_2\text{FeCoO}_6$ activates peroxymonosulfate heterogeneously, with its heterogeneity being more pronounced at neutral pH. Kinetics studies reveal that BPF degradation obeys pseudo First order kinetic with an activation energy of 14.085 KJ/mol and an apparent rate constant of 0.026 min^{-1} . Under conditions of 0.45 g L^{-1} and 10^{-4} M PMS, the complete BPF degradation occurred within 90 min at neutral conditions. In addition, the degraded BPF had undergone more than 65% mineralization within 6 h. The combination of UV irradiation (254 nm) with the $\text{Sr}_2\text{FeCoO}_6$ -PMS system induces a potential acceleration in the mineralization rate. The effects of humic acid, carbonate, bicarbonate and chloride were also evaluated. A total of 8 products were detected, and the associated degradation pathway was proposed. To identify the dominating reactive species generated in the $\text{Sr}_2\text{FeCoO}_6$ /PMS system, radical quenching tests and in situ electron paramagnetic resonance analysis were performed. To our knowledge, this is the first study that documents the heterogeneous activation of peroxymonosulfate with cobalt-iron based double perovskite for the treatment of the new emergent compound Bisphenol F.

1. Introduction

Bisphenol A (BPA), considered as the representative of EDCs (endocrine disrupting chemicals), has been widely used for the production of variety of chemical materials such as polycarbonate plastic and epoxy resins [1–4]. Faced with increasing concern due to its potential adverse human health impacts, BPA has been banned in certain products in many countries, such as Canada, china and in the European Union [5,6]. Using substitution of BPA for manufacturers to comply with the new regulations is consequently necessary. Bisphenol-F (4,4

-dihydroxydiphenylmethane, BPF) is now widely used in various industrial applications and considered as a “safer” alternative to BPA due to its excellent thermostability and photostability [7–9]. Despite this stability, the occurrences of BPF in environmental matrices have been frequently reported in the past three years. The potential adverse effects of BPF on humans have been uncovered by many researchers [10–16]. Therefore, it is necessary to take action for the removal of BPF from aquatic environment.

Advanced oxidation processes (AOPs) have been widely investigated as an efficient technique for the degradation of recalcitrant

* Corresponding authors at: Laboratory of Green Chemistry, School of Engineering Science, Lappeenranta University of Technology, Sammonkatu 12, FI-50130 Mikkeli, Finland.
E-mail addresses: samiabenhammouda@gmail.com (S.B. Hammouda), mika.sillanpaa@lut.fi (M. Sillanpää).

organic contaminants in water environment. The AOPs may be inherently hampered by the short lifetime of hydroxyl radicals $\cdot\text{OH}$ ($< 1 \mu\text{s}$) [17,18]. Over the last decade, sulfate radicals based advanced oxidation processes (SR-AOPs) have gained increasing attention from scientists as an innovative non-selective oxidative water treatment technique [19–23]. Sulfate radical ($\text{SO}_4\cdot^-$), with a redox potential of 2.5 to 3.1 V, has become an alternative to the hydroxyl radicals. $\text{SO}_4\cdot^-$ is a strong one-electron oxidant, but it also readily reacts by addition to C–C double bonds and by H-abstraction [24]. Besides its higher redox potential, $\text{SO}_4\cdot^-$ offers other advantages with respect to $\cdot\text{OH}$, such as wider working pH range (2–8) and higher life time (30–40 μs) [24–30]. Commonly, peroxymonosulfate (PMS) and persulfate (PS) are the main peroxides used for the $\text{SO}_4\cdot^-$ production [31–34]. Heat, UV irradiation and transition metals ions can all excite PMS and PS to form $\text{SO}_4\cdot^-$ [35]. Among those ways, the introduction of transition metals appears to be an inexpensive and practical method for oxidant activation. PMS, with an asymmetric structure ($\text{HO}-\text{O}-\text{SO}_3^-$) and a longer superoxide O–O bond ($l_{\text{O}-\text{O}} = 1.326 \text{ \AA}$) is believed to be more easily activated by transition metals to generate $\text{SO}_4\cdot^-$ than PS, which possesses a symmetric structure ($^-\text{O}-\text{O}-\text{SO}_3^-$) and a more compact O–O bond ($l_{\text{O}-\text{O}} = 1.322 \text{ \AA}$) [36–38]. Several metals have been tested for the PMS activation by Dionysiou and co-workers [20,39] and it has been concluded that cobalt ions (Co^{2+}) have the highest reactivity. Nevertheless, considering its carcinogenic potential, using cobalt as a homogeneous catalyst is not recommended for practical applications [40]. Hence, to avoid this risk, the development of stable heterogeneous catalysts containing cobalt for PMS activation has become a top priority [41–43]. Unsupported and supported cobalt oxides on other metal oxides or carbon substrates were reported as effective heterogeneous catalysts for PMS activation [44–49]. Bismuth-cobalt oxides Co_3O_4 - Bi_2O_3 and cobalt-containing spinel oxides such as CoFe_2O_4 and CuCo_2O_4 have been also reported to present a high activity for PMS decomposition owing to a synergistic effect of the redox couples between the different metal components [50–53].

Recently, special attention has been paid by our research group to the development of novel perovskite based catalysts for water treatment by means of advanced oxidation processes [54,55]. The perovskite oxides with a typical ABO_3 structure, where A sites are larger-sized alkali and rare earth metals and B sites are 3d transition metal ions, are capable of hosting more than 90% of metal elements in the periodic table [38,56,57]. From our previous studies, it was demonstrated that ABO_3 -type perovskites could be considered promising catalysts for wastewater treatment. Interestingly, the single nanostructured cobalt based-perovskite oxides ACoO_3 (A = La, Ba, Sr and Ce) have shown good reactivity in PMS activation for phenol degradation through SR-AOPs.

LaCoO_3 perovskite has also been applied by Pang et al. [58] to generate sulfate radicals from PMS for rapid mineralization of 2-phenyl-5-sulfobenzimidazole acid. Lin et al. [59] have further investigated the LaMO_3 perovskites (M = Co, Cu, Fe and Ni) in the Rhodamine B decolorization and it has been reported that LaCoO_3 exhibited the best catalytic activity, confirming the critical role of cobalt in PMS activation. Although most of the previous investigated single perovskite showed good activities towards oxidative processes, the lack of magnetism is a problem for the post-separation phase.

More recently, double iron based perovskite with the formula AFeBO_6 have received a great deal of attention due to their high stability and strong magnetic properties. Attractively, their use for water treatment applications and reactivity towards PMS has never been investigated.

Herein, cobalt-iron based strontium trimetallic oxide was synthesized with the citric acid gel method and used as catalyst for PMS activation, with Bisphenol F, as the target pollutant. The catalyst was characterized by means of nitrogen isotherm adsorption, scanning electron microscopy, X-ray photoelectron spectroscopy and X-ray diffraction. The reactivity of the magnetic double perovskite for PMS

decomposition was compared with that of the single perovskite catalysts SrFeO_3 and SrCoO_3 . A synergistic effect between $\equiv\text{Co}$ and $\equiv\text{Fe}$ was identified. The effectiveness of the double perovskite and PMS combination was studied varying PMS concentration, catalyst dosage, solution pH and temperature, which are the main operating variables. Cobalt and iron leaching was also considered at different operating pHs. The influence of water matrix components on the removal efficiency was also examined. The generation of $\text{SO}_4\cdot^-$ radicals was elucidated by conducting experiments using various radical scavengers and electron paramagnetic resonance (EPR) measurement. Possible pathway of the Bisphenol F degradation was proposed, and the mechanism for PMS activation on the surface of $\text{Sr}_2\text{FeCoO}_6$ was also discussed. Lastly, mineralization of BPF by UV/ $\text{Sr}_2\text{CoFeO}_6$ /PMS process was also assessed. The obtained data could provide useful information on the applicability of UV/ $\text{Sr}_2\text{CoFeO}_6$ /PMS based AOPs for the treatment of water contaminated with BPF or other organic compounds. Catalyst reusability has also been assessed.

2. Experimental

2.1. Chemicals

All chemicals used in this study were reagent grade or higher and purchased from Sigma-Aldrich. All solutions were prepared using deionized water (resistivity 18.2 M Ω , arium pro system). In this study, the Potassium peroxymonosulfate (KHSO_5) has been used as oxidant.

2.2. Catalysts synthesis

$\text{Sr}_2\text{FeCoO}_6$ was prepared via the classic sol-gel citrate and calcination approach [60]. Appropriate amounts of cobalt, strontium and iron nitrates were dissolved in deionized water to form a homogeneous solution. After stirring continuously for 2 h, the stoichiometric amount of citric acid required to form citrate with all the metals ions was further added to the above solution and followed by an additional heating-stirring step of 12 h over 100 °C to evaporate water and produce the desired gel. The resultant sol-like solution was then dried for 24 h at 80 °C. The obtained resin was then grinded into fine powders and calcined at 700 °C in air for 5 h to remove the organic species and to be transformed into a uniformly mixed metal oxide with a perovskite crystal structure. Single perovskites: SrFeO_3 and SrCoO_3 were also prepared for comparison in a way almost identical to that reported in previous studies [54,55].

2.3. Catalyst characterization

The X-ray powder diffraction spectra of the catalyst was recorded on a PANalytical Empyrean diffractometer with a Co-K ($= 1.7809 \text{ \AA}$) X-ray radiation source operated at 40 kV and 40 mA. The surface morphology of the catalyst was characterized using were carried out using emission scanning electron microscope (SEM). The elemental composition of the double perovskite was determined using (EDX) as a qualitative analysis technique. The EDX analysis was performed at several points and averaged to obtain the representative results.

Nitrogen adsorption/desorption experiment were used for textural studies with Micromeritics' TriStar II PLUS instrument. All the studied samples were pre-degassed in vacuum at 200 °C for 2 h. Specific surface area were determined using the classical BET model. The study of the surface composition and the electronic states of elements in the valence-band region of the double perovskite oxide were recorded on a ESCALAB 250 X-ray photoelectron spectroscopy (XPS) with Al-K (1486.6 eV) as the X-ray source.

Reactive oxygen species (ROS) were detected by electron spin resonance (ESR) spectroscopy using DMPO as a spin trap agent. The ESR spectra were recorded at room temperature using a quartz flat cell on a CMS-8400 paramagnetic resonance spectrometer under the following

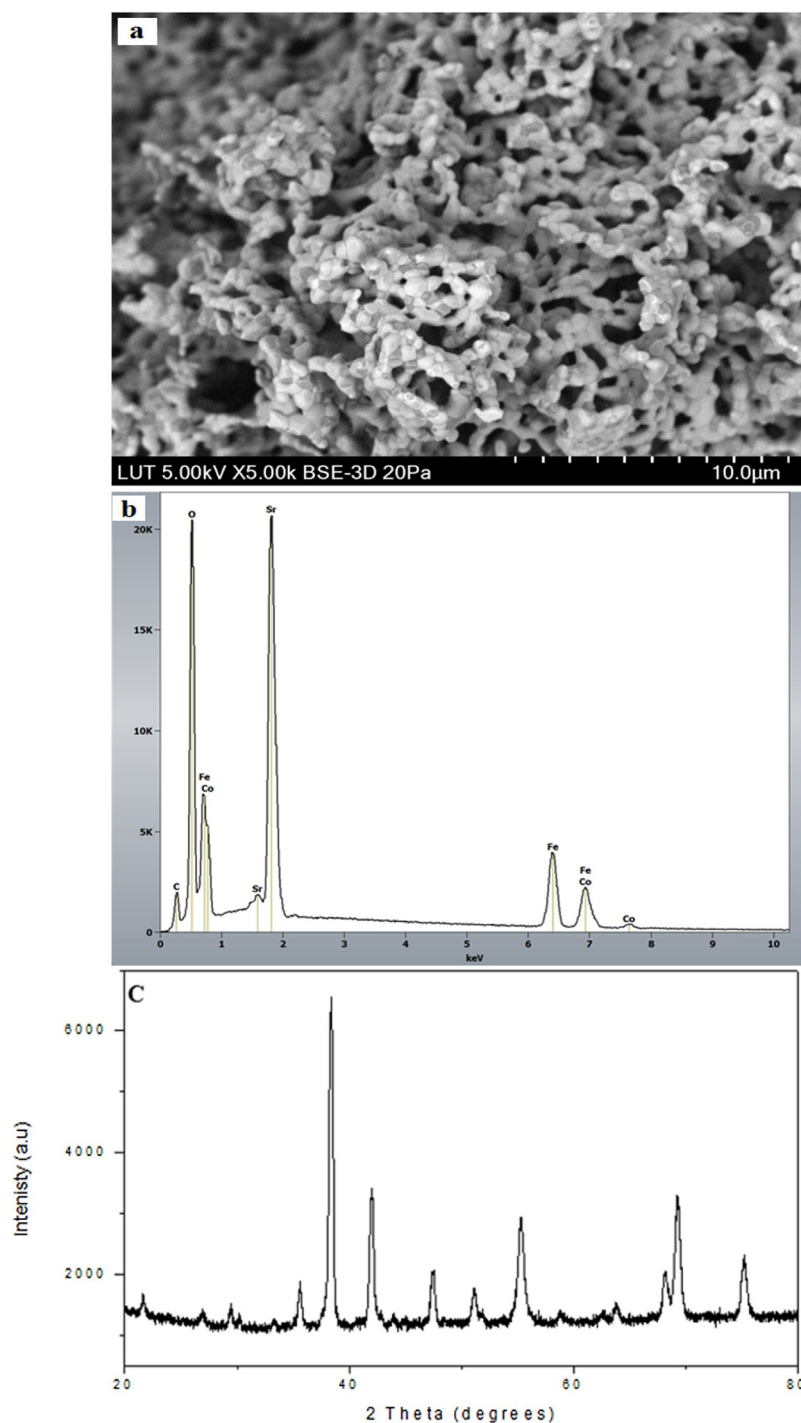


Fig. 1. a-SEM micrograph of the synthesized $\text{Sr}_2\text{FeCoO}_6$, b-Energy dispersive X-ray spectroscopy (EDS) spectra acquired in scanning electron microscopy (SEM) at the top view sample of $\text{Sr}_2\text{FeCoO}_6$, Acc voltage 15Kv, Scale bars are 5 μm . c- X-ray diffraction patterns of $\text{Sr}_2\text{CoFeO}_6$ double perovskite, space: Pbnm; crystal structure: monoclinic with $\alpha = \gamma = 90^\circ$, $\beta = 125^\circ$, $a = 9.604 \text{ \AA}$, $b = 5.560 \text{ \AA}$, and $c = 5.545 \text{ \AA}$.

conditions: magnetic field $336.5 \pm 6.0 \text{ mT}$ width, power attenuation 10 dB, field modulation 0.100 mT, sweep time 100 s, microwave frequency 9450 MHz.

2.4. Experimental procedure

The Bisphenol F treatment was conducted by batch type experiments. Typically, the required amount of catalyst was added firstly to 100 mL of BPF solution with an initial concentration of 20 mgL^{-1} and then a known concentration of PMS was added to the solution to initiate

the reaction; meanwhile mechanical stirring was kept to ensure a homogeneous solution throughout the reaction. Periodically, samples were withdrawn from the reactor and filtered immediately via a $0.45 \mu\text{m}$ membrane. The BPF degradation kinetics was described by using the pseudo-first order model.

Radical quenching studies were performed to determine the type of active radical generated in the reaction. Two different kinds of quenching reagent, viz. methanol and *Tert*-butyl alcohol, were used for the study.

Table 1
Textural properties of $\text{Sr}_2\text{FeCoO}_6$.

Catalyst	BET surface area ($\text{m}^2 \text{g}^{-1}$)	Pore volume ($\text{m}^3 \text{g}^{-1}$)	Pore size (nm)
$\text{Sr}_2\text{FeCoO}_6$	2.36	0.002	7.32

2.5. Analytical methods

Bisphenol F concentration was measured by a Shimadzu High Performance Liquid Chromatography equipped with UV detection (HPLC-UV) using a Kinetex column C18 (5 m, 4.6×150 mm). A mobile phase composed by 20 mM (phosphoric acid) potassium buffer solution (pH 2.5) (A) and acetonitrile (B), with an isocratic percentage composition of 70:30 A:B. The UV detector wavelength was set at 229 nm. The flow rate was set at 1.0 mL min^{-1} and the detection wavelength was at 229 nm. The retention time was around 6.80 min. A pseudo- first-order kinetics was adopted for the estimation of initial reaction rate constants.

The intermediates and by-products of BPF degradation were analyzed by a head space gas chromatography–mass spectrometry (GC–MS) (Agilent-GC 6890N, MS 5975) with Agilent DB-5MS GC column dimensions 30 m, 0.25 mm, 0.25 μm . The inlet temperature was 250°C in split less mode and the injection volume was $1.0 \mu\text{L}$. The oven temperature was programmed at 50°C for 3 min and it raises at the rate of 5°C/min to 300°C held for 2 min. Two different solid phase extraction (SPE) methods were investigated for switching the solvents as

well as to extract more generated intermediates in the samples that can be detected by GC–MS analysis. The reaction samples were extracted using strata X column and strata C18 and as extraction solvents, dichloromethane and methanol, respectively. Before injection, the derivatization of compounds in the extracted samples was performed using BSTFA/TMCS (*N,O*-Bis (trimethylsilyl) trifluoroacetamide/Trimethylchlorosilane) and MTBSTFA (*N-tert*-Butyldimethylsilyl-*N*-methyltrifluoroacetamide), respectively, at 50°C for 30 min [95].

Cobalt and iron release were quantified by means of atomic absorption using Thermo Scientific iCAP 6000 ICP. Generated carboxylic acids, oxalic, formic and acetic acids were identified and quantitatively followed by ion chromatography with suppressor equipped with a conductivity detector using a Shodex IC SI-50 4E (4.0 mm I.D. \times 250 mm). The eluent was 3.2 mM Na_2CO_3 and 1 mM NaHCO_3 at a flow rate of 0.7 mL min^{-1} . The mineralization of the BPF aqueous solutions during the treatment was monitored by measuring their non-purgeable organic carbon (NPOC) abatement. The NPOC in samples was quantified by a TOC analyzer purchased from Shimadzu. Organic carbon compounds were combusted and converted to CO_2 , which was detected and measured by a non-dispersive infrared detector (NDIR). Standard potassium hydrogen phthalate solutions were used as standards for the NPOC analysis.

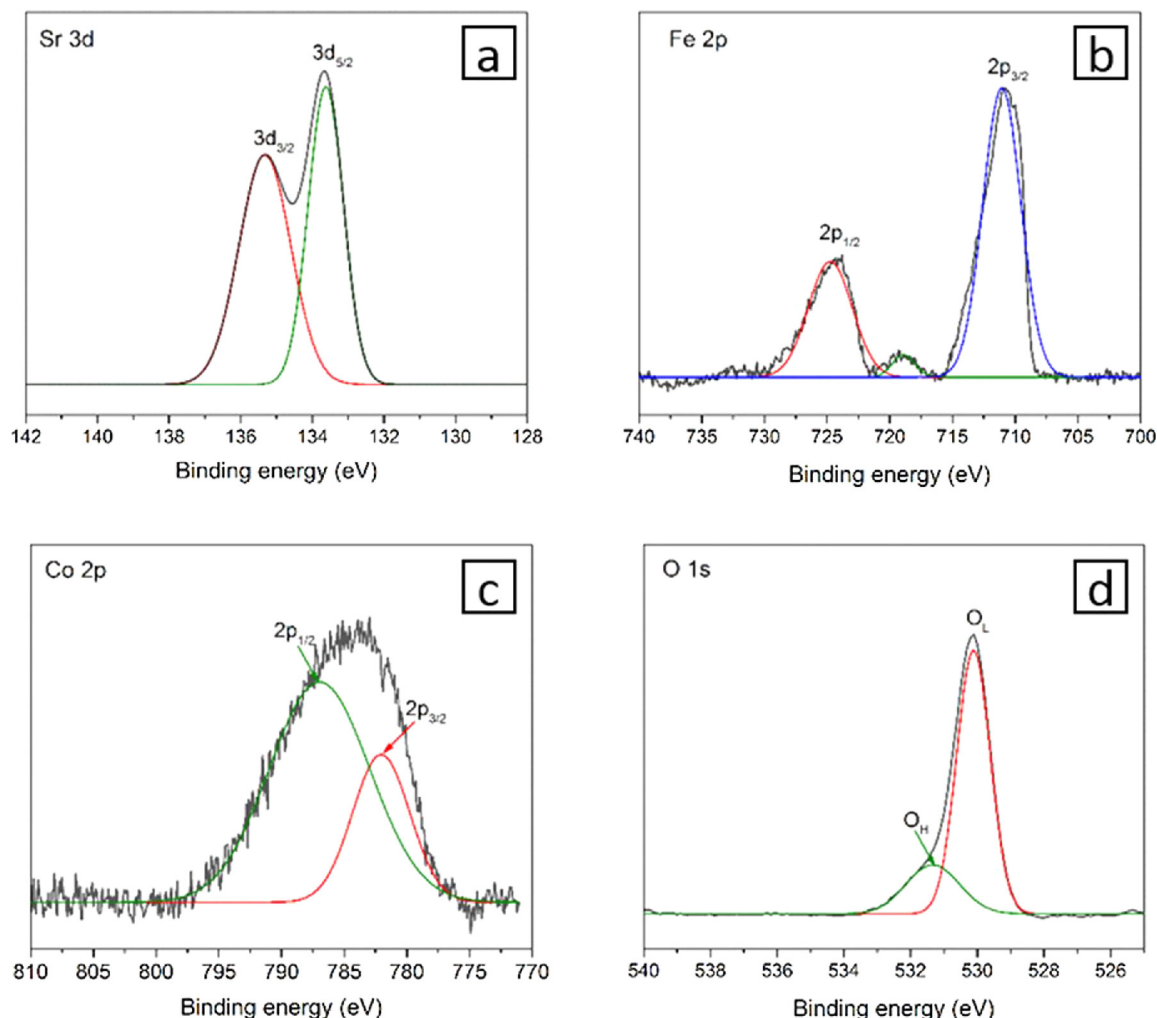


Fig. 2. High resolution XPS spectra of a- $\text{Sr}3\text{d}$, b- $\text{Fe}2\text{p}$, c- $\text{Co}2\text{p}$ and d- $\text{O}1\text{s}$.

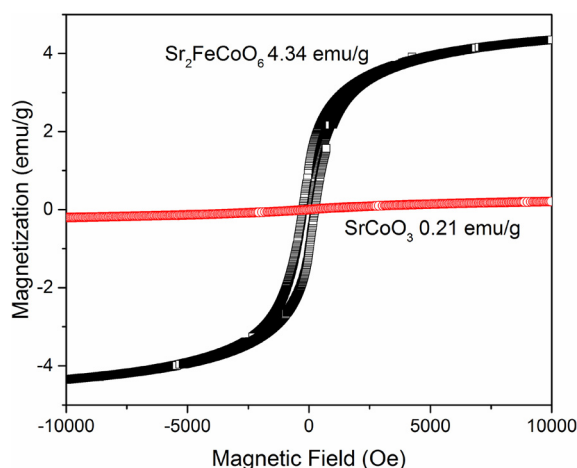


Fig. 3. Magnetization curves of $\text{Sr}_2\text{FeCoO}_6$ double-perovskite and SrCoO_3 ranging from -10,000 to 10,000 Oe at room temperature.

3. Results and discussion

3.1. Characterization of the magnetic catalyst $\text{Sr}_2\text{FeCoO}_6$

The microstructure of the double perovskite catalyst $\text{Sr}_2\text{CoFeO}_6$ is given in Fig. 1. A porous morphology formed through connected particles was obtained for the catalysts after being calcined at $700^\circ\text{C}/5\text{ h}$. The EDX spectra indicate the presence of the constituent elements (Sr, Fe, Co and O). The weak carbon signal observed at around 0.2 Kev was ascribed to the spreading of the sample on carbon conductive tape for the EDX measurement.

The XRD pattern of the $\text{Sr}_2\text{CoFeO}_6$ double perovskite nanocrystals recorded at room temperature is also depicted in Fig. 1. The sharp and intense diffraction peaks in the scanning range (20° – 80°) indicate the high crystallinity and purity of the obtained double perovskite catalyst. The diffraction peaks at 35.608° , 39.389° , 41.989° , 47.442° , 51.131° , 55.283° , 68.110° and 69.253° were on a monoclinic unit cell with ordered Co and Fe atoms (space group = $\text{P}121/\text{c}1$) with $\alpha = \gamma = 90^\circ$, $\beta = 125^\circ$, $a = 5.482\text{ \AA}$, $b = 5.531\text{ \AA}$, and $c = 9.504\text{ \AA}$, respectively). The ideal structure of this double-perovskite can be viewed as a regular arrangement of corner-sharing FeO_6 and CoO_6 octahedra alternating along the three crystal directions.

The nitrogen adsorption/desorption measurements were also carried out to determine the specific surface area and characteristics porosity of $\text{Sr}_2\text{FeCoO}_6$ as summarized in Table 1. The BET surface area of $\text{Sr}_2\text{FeCoO}_6$ was found to be $2.3\text{ m}^2\text{ g}^{-1}$, with corresponding volume of $0.002\text{ cm}^3\text{ g}^{-1}$.

XPS was employed to investigate the surface properties of the $\text{Sr}_2\text{FeCoO}_6$ double-perovskite and the chemical environments of Sr, Fe, Co, and O, which were simulated by Gaussian curve-fitting of the Sr 3d, Fe 2p, Co 2p, and O 1s spectra. The XPS spectra (Fig. S1) and fitting results are presented in Fig. 2, where the gray lines are the obtained spectra and the colored lines present the fitted curves. The Sr 3d core-level spectrum (Fig. 2.a) shows two peaks at binding energies (BE) of 133.3 and 135.1 eV could be assigned to Sr $3\text{d}_{5/2}$ and $3\text{d}_{3/2}$ respectively. The BE gap between these two species is 1.8 eV , which is close to the third layer electronic spin-orbit splitting of Sr (1.7 eV), suggesting that the predominant chemical valance state of Sr in the as-prepared double-perovskite catalyst is $+2$ [61]. This indicated that the consistency of Sr in the as-prepared double-perovskite and the double-perovskite components could not be separated, i.e., the as-prepared double-perovskite is not physically consisted of two single single-perovskites of SrFeO_3 and SrCoO_3 . Similar conclusion has been reported in the other SrFeMoO_3 double-perovskite [62]. The fitting of Fe 2p curve (Fig. 2.b) found three BE peaks at 710.9 , 724.6 , and 718.8 eV , which

could be assigned to Fe $2\text{p}_{3/2}$, Fe $2\text{p}_{1/2}$, and the satellite peaks of Fe^{4+} species, respectively. These peaks were same as the Fe 2p peaks in the reported delafossite $\text{CuAl}_{1/2}\text{Fe}_{1/2}\text{O}_2$. In Co 2p fitting curve (Fig. 2.c) two BE peaks at 781.2 and 789.4 eV could be assigned to Co $2\text{p}_{3/2}$ and Co $2\text{p}_{1/2}$, respectively. No noticeable shoulder peak was observed in Co 2p spectra, suggesting the cobalt in $\text{Sr}_2\text{FeCoO}_6$ double-perovskite is predominantly in the state of $+4$. The BE gap between Co $2\text{p}_{3/2}$ and Co $2\text{p}_{1/2}$ is 8.2 eV , which is lower than the value of the reported single-perovskite LaCoO_3 [63], revealing the lower second layer electronic spin-orbit splitting in the $\text{Sr}_2\text{FeCoO}_6$ double-perovskite. This might be attributed to the presence of iron in the double-perovskite, resulting in positive superexchange interaction between Co (B) and Fe (B') [64]. According to the method reported by Falcon et al. [65], the Sr/Fe/Co atomic ratio in $\text{Sr}_2\text{FeCoO}_6$ double-perovskite was calculated to be $1.94/1.06/1$ in the basis of the intensities of Sr $3\text{d}_{5/2}$, Fe $2\text{p}_{3/2}$ and Co $2\text{p}_{3/2}$ peaks. The Sr/Fe/Co ratio is very close to the stoichiometric Sr/Fe/Co = $2/1/1$, further proving the integration of the double-perovskite.

Finally, the fitting curve of O 1s core-level spectrum (Fig. 2.d) shows two obvious peaks with BE of 529.2 eV and 531.5 eV . The relatively stronger peak at 529.2 eV is the characteristic peak of perovskite lattice oxygen (O_L) [66], while the other peak at 531.5 eV could be assigned to the presence of hydroxyl groups adsorbed on the surface of the double-perovskite in the atmosphere environment [66].

The magnetization curves of the $\text{Sr}_2\text{FeCoO}_6$ double-perovskite and SrCoO_3 single-perovskite were measured by a vibrating sample magnetometer (VSM) at room temperature. The obtained results are illustrated in Fig. 3. It is obviously noticed that the saturation magnetization of $\text{Sr}_2\text{FeCoO}_6$ double-perovskite (4.34 emu/g) was much higher than that of the SrCoO_3 single-perovskite (0.21 emu/g). The obtained saturation magnetization of $\text{Sr}_2\text{FeCoO}_6$ double-perovskite is in a good agreement with the literature ($\text{Sr}_2\text{FeMoO}_6$ [67] and $\text{Sr}_2\text{FeFeO}_6$ [68]). Normally, the family of double perovskites has the general formula $\text{A}_2\text{BB}'\text{O}_6$, where A is alkali metal or lanthanides, and B and B' are transition metals. Each B/B' atom is surrounded by an oxygen octahedron and A encaged in holes produced by eight adjacent oxygen octahedron [69]. Orayech et al. [70] have explained that the main magnetic property of double perovskites are due to the competition between ferromagnetic and anti-ferromagnetic interactions and a spin-orbit coupling of Co in the octahedral coordination. The occupied high-spin band mainly consists of Fe 3d electrons forming the localized spins on the Fe sites, while the low-spin band is mainly occupied by hybridized Fe 3d and Co 2d, leading to interact ferromagnetically through the Fe-O-Co super exchange path, which was mentioned in XPS. The magnetic ability endows the $\text{Sr}_2\text{CoFeO}_6$ double-perovskite easy separation in practical application.

3.2. Catalytic activity and structural stability of the magnetic double perovskite

The reactivity of the prepared double perovskite oxide as the catalyst for PMS activation was evaluated through the degradation of Bisphenol F. Comparative experiments were performed in different systems.

Prior to the catalytic assays, controls tests were firstly performed in the absence of oxidant and/or catalyst in order to examine the possible contribution of adsorption phenomena and the possible direct oxidation by PMS. From Fig. 4, it is obviously seen that, without PMS, less than 10% of BPF was removed from the aqueous solution within 120 min of treatment, suggesting the weak affinity between the BPF molecules and the surface catalyst. Thus, the adsorptive removal of BPF could be neglected. Another control test was conducted in the presence of PMS and absence of $\text{Sr}_2\text{CoFeO}_6$. Results showed about 22% removal of BPF within 120 min of treatment. The low impact of PMS alone was expected. In fact, although PMS is thermodynamically a strong oxidant, its direct reaction with the majority of the pollutants is too slow so that activation is required.

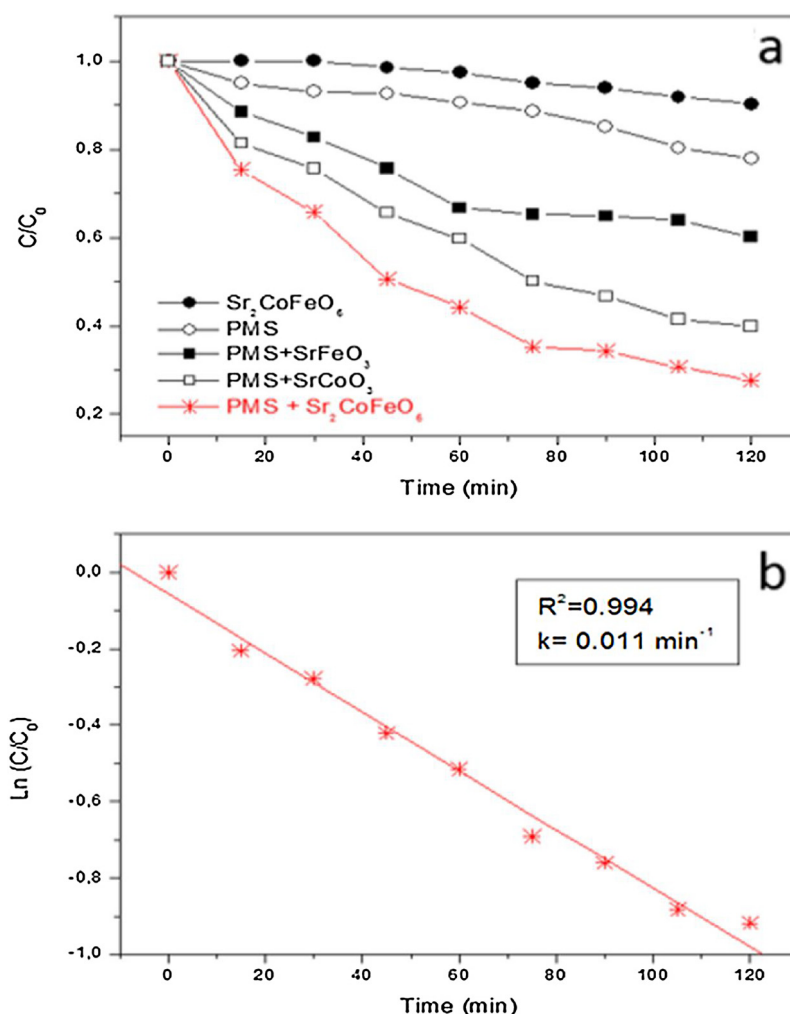


Fig. 4. a. Adsorptive behavior of Bisphenol F (Experimental conditions: Catalyst loading 0.3 g L^{-1} , without pH adjustment, $[\text{Bisphenol F}]_0 = 20 \text{ mg L}^{-1}$, working volume = 100 mL, and its degradation behavior under PMS and Catalyst/PMS system (Experimental conditions: $[\text{PMS}] = 10^{-4} \text{ M}$, Catalyst loading 0.3 g L^{-1} , without pH adjustment, working volume of 100 mL, $[\text{Bisphenol F}]_0 = 20 \text{ mg L}^{-1}$). b. Kinetic behavior under the heterogeneous Sr_2CoFeO_6 /PMS system.

Subsequently, the catalytic potential of the double magnetic catalyst Sr_2CoFeO_6 and the single perovskite catalysts $SrMO_3$ ($M = \text{Fe, Co}$) was assessed in the heterogeneous system with an initial PMS concentration of 10^{-4} M , a catalyst dosage of 0.3 g L^{-1} and without pH adjustment. With Sr_2CoFeO_3 , a great improvement on the BPF conversion efficacy was observed leading to over 72% removal efficiency within 120 min of reaction. As can be seen from Fig. 4.a the activities of the three investigated catalysts were in an order of Sr_2CoFeO_3 (72.35%) > $SrCoO_3$ (69.10%) > $SrFeO_3$ (39.85%).

The above results suggest that the metallic sites were essential for PMS activation. The degradation of BPF by Perovskite/PMS system obeyed pseudo-first order reaction kinetics ($\ln(C/C_0) = -kt$ (Fig. 4.b)). The apparent first order rate constant for the BPF removal at its initial concentration of 20 mg L^{-1} , varied from 0.004 min^{-1} to 0.011 min^{-1} . As illustrated in Fig. 4.b, the degradation of BPF through Sr_2CoFeO_3 was perfectly fitted by the pseudo first order model with a regression coefficient of 0.994. The best performance was obtained with this catalyst which was therefore selected for further more detailed investigation of BPF degradation under various experimental conditions. Beside its higher performance, the good dispersibility and magnetic recyclability of Sr_2CoFeO_3 would also facilitate its recovery and practical application. After treatment, the catalyst particles could be easily collected by using a magnet.

It is well known that the oxidation of organic compounds through PMS activation process is strongly affected by the solution pH [71–73].

As stated in the interesting work of Solis et al [74] dedicated to the degradation of organic compounds by single based perovskite catalyst, one of the major inconveniences in using this heterogeneous catalyst was its deactivation due to the release of transitions metal to bulk solution. Moreover, this metallic leaching may result in misleading interpretation. Solis et al. reported that acidic reaction conditions favored the dissociation of the solid catalyst and relatively high concentration of 4 mg L^{-1} of cobalt was released from LaCoO_3 perovskite surface, concluding that the homogeneous reaction predominates over the heterogeneous path. The negative impact of acidic pH on the catalyst stability was also been pointed out in our previous investigation [54] of the phenol degradation by heterogeneous monopersulfate activation on nanostructured cobalt based-perovskite catalysts ACoO_3 ($A = \text{La, Ba, Sr}$ and Ce).

Accordingly, herein, an experimental series was performed under various pH conditions. Besides the BF degradation, the leached amount of cobalt and iron was also monitored in these assays.

As observed in Fig. 5.a, the system is more effective at low pH. At pH 3, total conversion of BPF was reached in 90 min. The rate of BPF decreased from 0.0349 min^{-1} to 0.0062 min^{-1} with increasing initial pH from 3 to 9. Expectedly, a significant leaching of cobalt (0.59 mg L^{-1}) and iron (0.48 mg L^{-1}) to water bulk was detected in the Sr_2CoFeO_6 /PMS when the working pH was 3 (Fig. 5.b).

In order to examine the homogeneous contribution of the metals leached at pH 3 from Sr_2CoFeO_6 to the overall heterogeneous PMS/

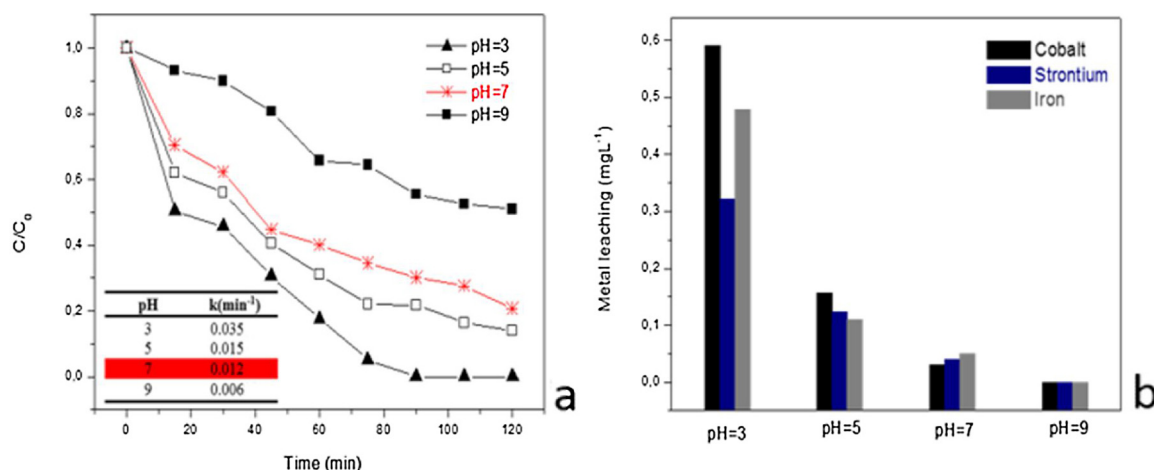


Fig. 5. Oxone mediated removal of Bisphenol F in the presence of Sr₂CoFeO₆: Effect of pH on a- the removal efficiency, b- the catalyst stability. Experimental conditions: [PMS] = 1.0 × 10⁻⁴ M, Catalyst loading 0.3 g L⁻¹, working volume of 100 mL, [BPF]₀ = 20 mg L⁻¹.

Sr₂CoFeO₆ reaction, a further test was performed. Sr₂CoFeO₆ nanoparticles were removed from the solution and the homogeneous reaction was conducted by addition of 10⁻⁴ PMS to the filtrate. Results showed that the homogenous Cobalt + iron/PMS reaction resulted in 42% BPF removal (the detailed results are not shown). This finding confirms that, at pH 3, the surface catalyzed process and the dissolved ions contribute together to the BPF remediation.

To prevent metal leaching and limit this study to the heterogeneous catalysis, experiments were performed at pH 7 using buffer solution (50 mM borate). As shown in Fig. 5, 70% of BPF was degraded by PMS activation with Sr₂CoFeO₆ (0.3 g L⁻¹) within 90 min, and the corresponding rate constant was about 0.0125 min⁻¹. Interestingly, as expected, the amount of cobalt and iron dissolved was quite low (below 0.05 mg L⁻¹ and 0.03 mg L⁻¹ for Co and Fe, respectively). The homogeneous contribution of metallic ions released from the solid catalyst was also analyzed at neutral pH by conducting an experiment in the presence of the metallic amount lixiviated at this pH. The results revealed that BPF removal was quite similar to that obtained in a blank run conducted with the PMS oxidant alone. Based on this observation, it can be proposed that the stability of the Sr₂CoFeO₆ would be better for higher pH.

Raising the initial pH to 9 causes a significant drop in BPF removal efficiency to about 46%. This behavior could be explained by the scavenging of sulfate radicals by hydroxyl radicals. These former possess weaker oxidation potential and shorter lifetime than SO₄•⁻. Another probable reason for the BPF efficiency decline at basic conditions is the self-decomposition of PMS. Above pH 7, the active oxygen of PMS starts to dissociate leading to decreased production of sulfate radicals [75,76].



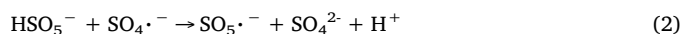
Moreover, it is important to note that, the point of zero charge is an elementary account of the surface of a metal oxide. The pH_{pzc} value of the catalyst was found to be 8.70. This explains the ability of the catalyst to adsorb anions, such as peroxymonosulfate HSO₅⁻, at acidic or neutral pH since its surface is positively charged. The low decomposition of peroxymonosulfate at pH = 9 could be ascribed to its second acid dissociation pK_a = 9.4.

Thus, after analyzing the trade-off between catalytic performances and leaching level, neutral pH, a compromise between leached metals and reaction rate, was chosen as the optimal pH for BPF oxidation.

An additional experimental series was conducted at different PMS concentrations by maintaining the rest of operating variables constant. According to the U.S. environmental protection agency, the maximum permissible limit of sulfate in drinking water is 250 mg L⁻¹ which

corresponds to around 400 mg L⁻¹ (0.65 mM) of PMS dosage [77,78]. Thus, the use of higher PMS concentration (> 0.65 mM) may induce secondary pollution by sulfate anions. Besides this risk, it is recommended for industrial applications to keep operating costs as low as possible by reducing the reagents consumption. In view of this, the study of the PMS impact on BPF degradation was limited in the range [0.05 mM–0.3 mM]. As depicted in Fig. 6.a, increasing PMS concentration from 0.05 mM to 0.1 mM showed a steep increase in BPF removal from 55.80 to 79.35% within 120 min. The rate of BPF degradation increased markedly from 0.006 to 0.012 min⁻¹. Further increase in PMS concentration up to 0.2 mM resulted in total removal of BPF within 120 min, the corresponding kinetic rate increase to 0.019 min⁻¹. No significant improvement in BPF removal efficiency was observed by a further raise in PMS concentration to 0.3 mM.

Theoretically, generation of reactive radicals would increase with the increase in PMS initial concentration, leading to a further enhanced degradation of BPF. However, a nonlinear kinetics, in respect to the linear increase in PMS concentration, was observed in the current study. This could be mostly ascribed to the fact that at higher concentration PMS itself can react with generated sulfate radicals (Eq. (2)), which in turn can reduce the degradation of target compound, BPF.



Anazi et al [79] also observed similar trend for 2-phenylbenzimidazole-5-sulfonic acid degradation using cobalt ferrite nanoparticles/PMS system in which further increase in oxidant concentration to 0.2 mM does not show any appreciable change in degradation efficiency. Thus, considering the trade-off between performance and cost, 0.2 mM PMS was chosen as optimal for BPF degradation.

To summarize, the above results indicated that Sr₂FeCoO₆ exhibited excellent ability to activate PMS for BF degradation, even at relatively low PMS concentration.

The influence of catalyst loading on Bisphenol F oxidation by Sr₂FeCoO₆-PMS process was also explored. As illustrated in Fig. 6.b, within 90 min, an obvious improvement in the removal efficiency, from about 64% to 100%, was observed when the catalyst dosage increased from 0.15 g L⁻¹ to 0.45 g L⁻¹. The corresponding kinetic rate increased from 0.011 to 0.026 min⁻¹. This improvement is mainly attributed to the availability of more catalytic ≡Co and ≡Fe sites that could behave as active sites on the catalyst surface, promoting the PMS activation and production of higher amount of free reactive oxygen species. This result demonstrates the crucial role of the Sr₂FeCoO₆ solid catalyst in the radicals' production. While with a further dosage increase from 0.45 to 0.6 g L⁻¹, no significant difference in the degradation performance occurred. This can be related to the agglomeration of nanoparticles

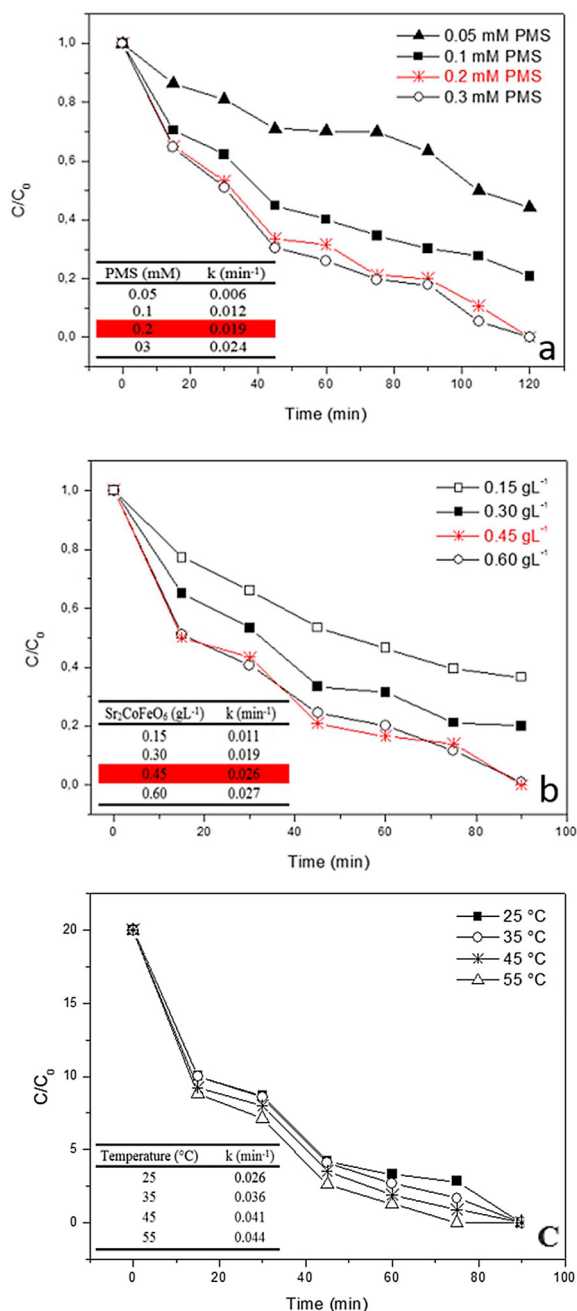


Fig. 6. PMS mediated removal of Bisphenol F in the presence of Sr₂CoFeO₆. a- Influence of PMS concentration. Experimental conditions: pH 7, Catalyst loading 0.3 g L⁻¹, working volume of 100 mL, [BPF]₀ = 20 mg L⁻¹. b- Influence of Catalyst concentration. c- influence of the temperature.

and/or to the consumption of the available SO₄·⁻ and ·OH free radicals scavenging by the excessive level of ≡Fe and ≡Co sites.

The temperature impact on BPF degradation was also investigated. From Fig. 6.c, the temperature increase was accompanied, as expected, by an enhancement on the BPF removal efficiency. The reaction rate constants were 0.026, 0.036, 0.041 and 0.044 at 25, 35, 45 and 55 °C respectively. Besides the enhancement of pollutant diffusion and adsorption, the positive effect of temperature could be related to the thermal activation of PMS at higher temperature as shown in Eq. (3).



On the basis of the Arrhenius equation (Eq. (4)), the apparent activation energy was estimated to be 14.085 kJ mol⁻¹, suggesting that

the reaction is diffusion controlled.

$$k = A \exp(-E_a/RT) \quad (4)$$

Where A is the Arrhenius constant, E_a (kJ mol⁻¹) is the apparent activation energy, R is the ideal gas constant (0.0083 kJ mol⁻¹ K⁻¹) and T (K) is the solution temperature.

3.3. Identification of reactive species

It is generally assumed that SR-AOPs are characterized by the possible coexistence of SO₄·⁻ and ·OH. According to the literature, the PMS activation with metals transition tends to generate mainly sulfate, peroxysulfate (SO₅·⁻) and hydroxyl radicals [80,81]. ·OH radicals may be formed through the reaction of sulfate radicals with H₂O (Eq. (5)) [82]. A small extent of SO₅·⁻ is generated simultaneously, however its activity is too low to be considered for taking part in the oxidation process [83].



Typically, SO₄·⁻ and ·OH radicals would oxidize BPF through different pathways. The ·OH radicals mainly attack organic compounds via addition to unsaturated bonds and H-abstraction, while SO₄·⁻ are more likely to react via electron-transfer mechanism [17,84,85]. Considering the difference in their attack pathway, it's mandatory to identify the major reactive specie involved in the overall PMS/Sr₂CoFeO₆ process.

Thus, radical quenching experiments were conducted by using two specific probe scavengers, i.e. *tert*-butyl alcohol (t-BuOH) and methanol. The alcohol lacking α-hydrogen t-BuOH was widely reported as a typical ·OH scavenger, as the rate constant for ·OH species (3.8–7.6 × 10⁸ M⁻¹ s⁻¹) is 3 orders of magnitude higher than that for SO₄·⁻ species (4–9.1 × 10⁵ M⁻¹ s⁻¹) [86,87]. Methanol, which has similarly high reactivity towards ·OH and SO₄·⁻, with rate constant of 9.7 × 10⁸ M⁻¹ s⁻¹ and 1.0 × 10⁷ M⁻¹ s⁻¹, respectively, is commonly used as a specific probe scavenger for both these radicals. [86–88].

Fig. 7 displays the rate of BPF oxidation under the influence of both quenching. As illustrated, the BPF degradation by Sr₂CoFeO₆ slightly decreases to 87.9% after the addition of t-BuOH scavenger, suggesting the minor contribution of ·OH in the overall BPF oxidation. However, under similar conditions, the addition of 0.1 M methanol resulted in a decreased BF removal to 47.5%. These results suggest that the main radical species produced during the PMS activation by the solid catalyst Sr₂CoFeO₆ was SO₄·⁻.

The contribution of SO₄·⁻ to the global Sr₂CoFeO₆/PMS process

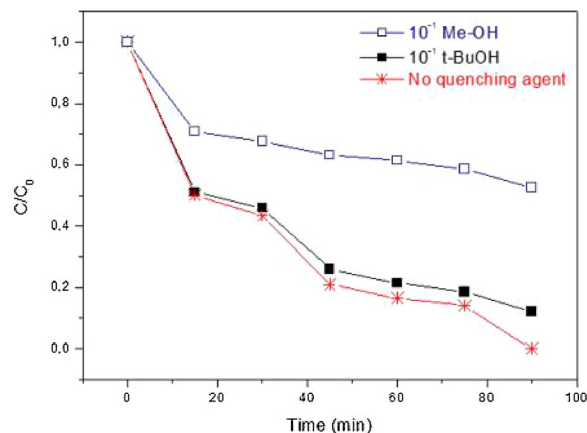
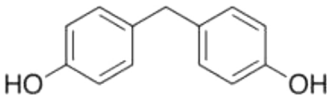
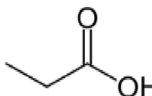
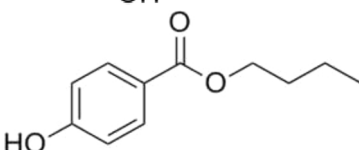
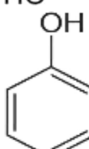
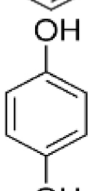
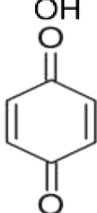
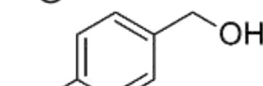
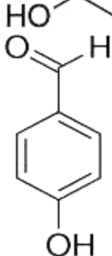


Fig. 7. Reaction quenching of BPF oxidation with Sr₂CoFeO₆ in the presence of methanol and *tert*-butyl alcohol. Experimental conditions: [PMS] = 1.0 × 10⁻⁴ M, Catalyst loading 0.3 g L⁻¹, pH 7, working volume of 100 mL, [BPF]₀ = 20 mg L⁻¹.

Table 2
Possible by-products formed during BPF oxidation.

Compound	Structure	MW
Bisphenol F		200
propanoic acid		74
Butylparaben		194
Phenol		94
Hydroquinone		110
Benzoquinone		108
4-Hydroxybenzyl alcohol		124
4-Hydroxybenzaldehyde		121
Unidentified compound	$C_{12}H_{15}O_3$	207

($\approx 88\%$) was determined by calculating the ratio between the removal efficiencies of the BF removal with and without $\cdot OH$ probe scavenger addition.

$$\% SO_4^{\cdot -} \text{ radicals contribution} = \frac{\%BF \text{ removal with (t-BuOH)}}{\%BF \text{ removal without (t-BuOH)}}$$

EPR spectroscopy using DMPO as trapping agent was also employed to determine the major specie involved in the SR-AOPs system. As shown in Fig. S2, in the presence of PMS and Sr_2FeCoO_6 , a seven-line peak in the EPR spectrum were observed, which conforms to the signals reported by Lin et al. [89] and Qian et al. [90] for DMPO- $SO_4^{\cdot -}$ adduct. This result allowed further confirmation of the predominant contribution of $SO_4^{\cdot -}$ rather than $\cdot OH$ radicals. This provides a direct evidence for the major formation of $SO_4^{\cdot -}$ radicals, however, a small

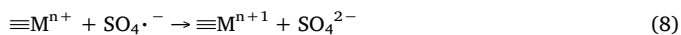
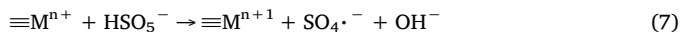
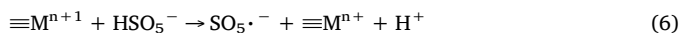
contribution of $\cdot OH$ radicals in the PMS system cannot be ruled out due to the slight decrease in the rate of BPF on addition of t-BuOH.

3.4. Reaction mechanism for the heterogeneous monopersulfate decomposition

PMS decomposition by reactions at heterogeneous catalyst surface is not well understood. However, it's well agreed that the heterogeneous catalytic decomposition of PMS is controlled by intrinsic reactions at the catalyst surface. Herein, the active species responsible for PMS activation and sulfate radicals production are M (M = Co, Fe). The BPF decomposition involves in the earlier step the adsorption of BPF molecules and PMS onto the perovskite surface through electrostatic interaction and π - π stacking. PMS activation can be achieved by a variety

of reactions, including mainly an oxidation-reduction process which involves the reduction of PMS by low-valent metals (M^{n+}).

Similarly to the Fenton and Fenton like systems, we propose that the rate-determining steps for the monopersulfate decomposition by the iron and cobalt-containing perovskite catalyst can be presented by the following reactions (Eqs. (6–8)):



Equivalently to hydrogen peroxide in the Fenton system where it can be both oxidized and reduced, monopersulfate could act as both an oxidant and reductant in the SR-AOPs systems.

As with the homogeneous system, it is believed that the mechanism of the heterogeneous catalysis, shown in Schema1, involves a one-electron transfer process [42]. One electron reduction of $\equiv M^{n+1}$ would result in the production of peroxy monosulfate anion radical ($SO_5^{\cdot-}$). It was already demonstrated by Anipsitakis and Dionysiou [39] that the latter transient species are too weak compared to sulfate radicals to induce pollutant oxidation. One electron donation by the low-valent metal $\equiv M^{n+}$ would result in the production of the highly active sulfate radical ($SO_4^{\cdot-}$), which could then initiate radical chain propagation reactions. By analogy to the Fenton reaction, we suggest that the surface reactivity of the envisaged catalyst is probably affected by the metals coordination. The overall reaction kinetic of monopersulfate decomposition is mainly affected by the extent of active surface sites and electron transfer rates.

3.5. Degradation pathway of bisphenol F

To the best of our knowledge, the BPF degradation mechanism by SR-AOPs has not yet been investigated. The mechanism of the BPF degradation through Sr_2CoFeO_6 -PMS was assessed and presented in this section. To elucidate the BPF pathway, the extract obtained from the reaction mixture using methanol as a solvent was subjected to GC-MS analysis. The GC-MS spectra of the extracted oxidation products were evaluated on the basis of literature information and mass fragmentation values. There were mainly eight reaction by-products detected in the present study. Fig. S3 exhibits the mass spectrum of the major detected compounds. Six of them were identified as phenol, propanoic acid, hydroquinone, benzoquinone, 4-Hydroxybenzyl alcohol and 4-hydroxybenzaldehyde (Table2). All of these identified compounds, except phenol and propanoic acid, have been detected previously in our work devoted to the oxidative degradation of BPF through the catalytic Fenton process. In this study, the exact radical reactions involved in the BPF attack cannot be distinguished with certainty because of the only detection of short chains in the reaction solution.

Though not identified in this work, due to the similarities in the reaction mechanism of $\cdot OH$ and $SO_4^{\cdot-}$ and based on our previous work, we speculate the formation of Bis(4-hydroxyphenyl) methanol, 4,4' dihydroxybenzophenone and 4-hydroxyphenyl 4-hydroxybenzoate, in the initial stages of oxidation. Further sulfate radicals attack results in weakening the C–C bond between two phenyl groups. The bond cleavage leads to the formation of phenol, hydroquinone, benzoquinone, 4-Hydroxybenzyl alcohol and 4-hydroxybenzaldehyde. Thereafter, the deprotonation and opening of the benzene rings results in the formation of propanoic acid and other short chain carboxylic acids. In this work, formic acid, acetic acid and oxalic acid were the main identified aliphatic byproducts. CO_2 and H_2O would be formed by further oxidation reactions. A plausible degradation pathway of BPF degradation is illustrated in Fig. 8.

3.6. Reactivity of spent Sr_2FeCoO_6 and reusability

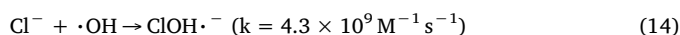
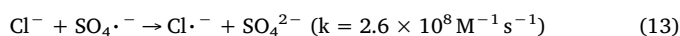
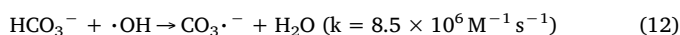
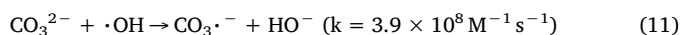
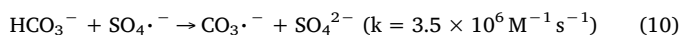
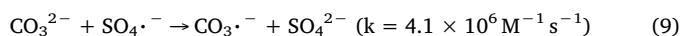
Fig. 9 exhibits the catalytic activity of the recycled Sr_2FeCoO_6 for BF degradation. As seen, the catalyst performance remained practically unaffected in the second and third round use and slightly decreased to about 87% in the fourth cycle. To evaluate the stability of Sr_2FeCoO_6 , the leaching of iron and cobalt was measured in the fourth recycled test. An ICP analysis indicated that leached amount of iron was about 0.09 mg L^{-1} in the system, while no cobalt was found in the solution. This result suggests that the cobalt and iron ions were strongly bonded in the perovskite framework, making it quite stable performance in the reaction.

3.7. Effect of co-existing water matrix chemicals

The presence of natural organic matter (NOM) in water and wastewater has to be considered when applying remediation processes aimed at pollutant removal. In fact, it is largely assumed that NOM have a negative impact on oxidative techniques because they may act as scavengers of reactive species, e.g. hydroxyl radicals and sulfate radicals. Humic acid is commonly used as a representative of NOM. The impact of humic acid on the kinetics of BPF by Sr_2FeCoO_6 /PMS process is illustrated in Fig. 10. The addition of 10.0 mg L^{-1} humic acid decreased greatly the removal efficiency of Sr_2FeCoO_6 /PMS, i.e., from 100 (without HA) to 63% after 90 min, which could result from the scavenging effect of NOM towards $\cdot OH$ and $SO_4^{\cdot-}$. An increase of HA concentration to 20 ppm further increases the degree of inhibition to 51%. This result is consistent with the literature reports showing that efficiency of the UV/PMS system for atrazine removal decreased from 98% to 23% when 3.2 mg L^{-1} of humic acid was added to the reaction mixture. Sharma et al [91] have also reported similar trends in their work devoted to the oxidative removal of bisphenol A by UVC/PMS. At high concentration, HA compete with target pollutant for $SO_4^{\cdot-}$ and $\cdot OH$ radicals, thereby reducing their availability for the target oxidation.

Thus, we can conclude that, when applying catalytic PMS SR-AOPs, a pre-treatment aiming to remove organic matter should be considered in order to minimize the negative effects from those non-target compounds.

The presence of inorganic compounds in the water matrix has also been shown to greatly influence the removal efficiency of target pollutants. Herein, the effect of inorganic anions such as Cl^- , HCO_3^- and CO_3^{2-} on BPF removal by Sr_2FeCoO_6 /PMS process was studied, the presence of which led to different degrees of inhibition on the abatement percentage of BPF, as illustrated in Fig. 10. The presence of HCO_3^- or CO_3^{2-} induce a significant inhibitory effect probably due to scavenging of reactive radicals by these anions (reactions (9)–(14)) [92,93]. The higher inhibitory effect on BPF removal efficiency obtained with CO_3^{2-} is attributable to its higher reactivity with both radicals.



Contrary to HCO_3^- or CO_3^{2-} and despite its high reactivity towards $\cdot OH$ and $SO_4^{\cdot-}$, the presence of Cl^- exerted a negligible inhibitory effect on the efficiency of the Sr_2FeCoO_6 /PMS. This unexpected result is in a good accordance with the negligibly small adverse of Cl^- observed by Khan et al. [94] in their study devoted to the degradation of the pesticide lindane in UV/PMS system.

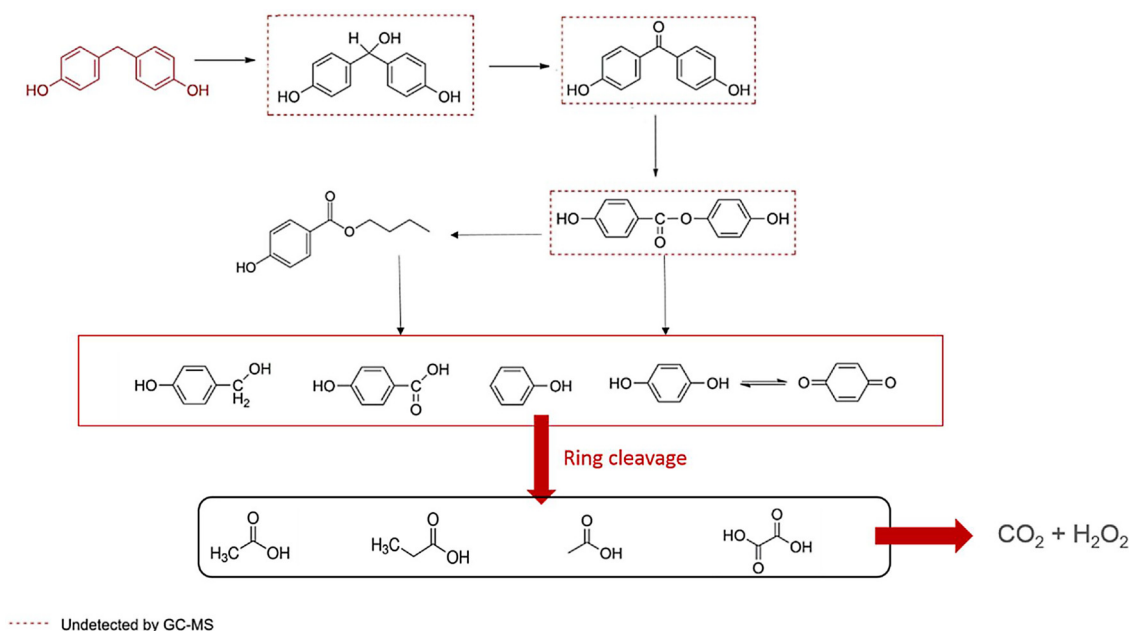


Fig. 8. Proposed pathway of BPF mineralization through $\text{Sr}_2\text{FeCoO}_6/\text{PMS}$ process.

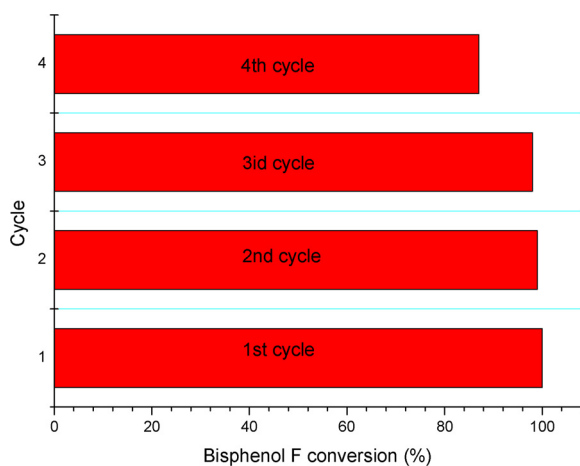


Fig. 9. Bisphenol F degradation in the tests of recycled $\text{Sr}_2\text{FeCoO}_6$ [0.3 g L^{-1} catalyst, 10^{-4} PMS, 20 ppm Bisphenol F and 25°C].

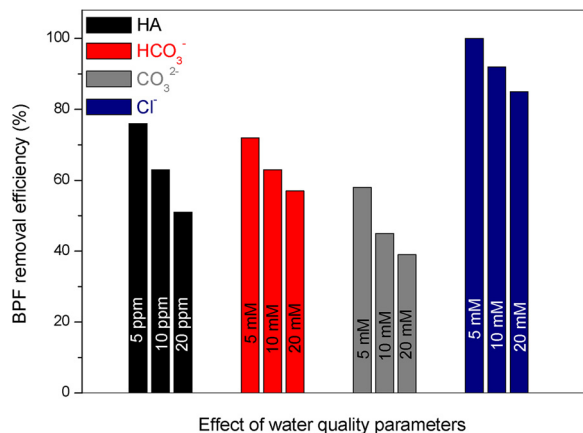


Fig. 10. Effect of humic acid or inorganic anions on the percentage removal of BPF in 90 min. $[\text{BPF}]_0 = 20 \text{ mg L}^{-1}$, $[\text{PMS}]_0 = 0.2 \text{ mM}$, $[\text{humic acid}]_0 = [5\text{--}20 \text{ mg L}^{-1}]$, $[\text{inorganic anions}]_0 = [5\text{--}20 \text{ mM}]$.

3.8. BPF mineralization

As shown above, BPF is initially converted to other organics by-products, mainly phenol, hydroquinone and benzoquinone, etc., which are all considered to be toxic to humans. The ultimate oxidation of BPF by means of sulfate radicals leads to the formation of organic acids via ring-cleavage and then mineralization to CO_2 . Therefore, it was considered to compare the efficiency of the envisaged process for the total organic carbon TOC abatement which might further suggest the removal of toxicity. The results of TOC removal are illustrated in Fig. 11. As can be seen, though much less effective than the removal of the parent compound, a 67% TOC removal by PMS/ $\text{Sr}_2\text{CoFeO}_6$ in 360 min was obtained. The rate of TOC removal was faster at the initial stage of the oxidation but slowed down with time, which could be attributed to the formation of persistent byproducts mainly oxalic, formic and acetic acids.

Some studies have demonstrated that the metallic catalytic decomposition of PMS assisted by UV irradiation metals can improve greatly the degradation and mineralization rate. Very recently Zeng et al reported the combined process with Fe(II) , PMS and UV as

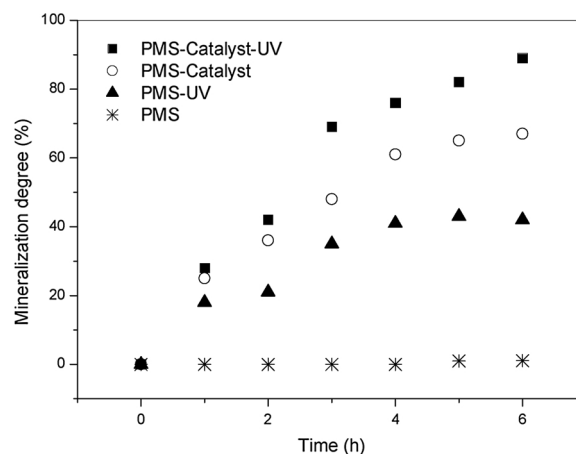


Fig. 11. Mineralization of Bisphenol F solution (20 mg L^{-1}) by $\text{Sr}_2\text{FeCoO}_6/\text{PMS}$ system (Experimental conditions [0.3 g L^{-1} catalyst, 10^{-4} PMS, 25°C]).

promising technology for the wastewater treatment. Therefore, in an attempt to further improve the BPF mineralization efficiency by producing more reactive radicals, UV irradiation ($\lambda = 254\text{ nm}$) was applied to the PMS-Catalyst reaction media. The UV irradiation would activate the PMS oxidant through hemolytic cleavage of the peroxide bond which results in the formation of both $\text{SO}_4^{\cdot-}$ and $\cdot\text{OH}$ radicals following the reaction below:



As seen in Fig. 11, the mineralization deficiency was significantly enhanced compared to the assay performed in the dark under similar conditions. An increase from 48 to about 69% after 3 h of treatment was observed when 0.45 g L^{-1} of catalyst were used in the presence of the light and PMS. This improvement could be ascribed as expected to the partial PMS decomposition due to UVA light absorption. Moreover, it should be noted that, after 6 h of irradiation, only about 7% of BPF was degraded through photolysis, indicating the high photo stability of BPF. For comparison purposes and under the same conditions, some non-promoted assays were also conducted. It can be seen that the mineralization efficiency has the following order UV/PMS /catalyst > PMS/Catalyst > PMS-UV > PMS.

4. Conclusions

The $\text{Sr}_2\text{FeCoO}_6$ magnetic catalyst was found to be effective for BPF oxidative degradation using peroxymonosulphate as oxidant for sulfate radical generation at pH 7. The envisaged magnetic catalyst presents stable performance in heterogeneous BPF oxidation for several runs. The BF oxidation follows zero-order kinetics with the activation energy of KJ/mol , according to Arrhenius definition. UV irradiation improves the catalytic mineralization of BPF. Neither direct UV photolysis nor PMS alone showed an apparent degradation. Eight byproducts from BPF degradation were identified using GC–MS analysis. Degradation pathway of BPF was also suggested based on the detected byproducts. Overall, $\text{Sr}_2\text{CoFeO}_6$ was shown to be a promising magnetic catalyst for water treatment at neutral conditions due to its easy recovery as well as the possibility of its subsequent reuse while maintaining its catalytic performance.

Acknowledgements

The first author would like to gratefully acknowledge Ms. Indu Imbat for conducting the GC–MS analysis and for providing advice during the extraction step. Dr. Ben Hammouda would like also to express her gratitude to Dr. Varsha Srivastava Ms. Sidra Iftikhar for providing guidance on the use of XRD and EPR, respectively.

Appendix A. Supplementary data

Supplementary material related to this article can be found, in the online version, at doi:<https://doi.org/10.1016/j.apcatb.2018.03.088>.

References

- [1] R. Kuruto-Niwa, Y. Terao, R. Nozawa, *Environ. Toxicol. Pharmacol.* 12 (2002) 27–35.
- [2] G.V. Korshin, J. Kim, L. Gan, *Water Res.* 40 (2006) 1070–1078.
- [3] P.E. Stackelberg, E.T. Furlong, M.T. Meyer, S.D. Zaugg, A.K. Henderson, D.B. Reissman, *Sci. Total Environ.* 329 (2004) 99–113.
- [4] A. Usman, M. Ahmad, *Chemosphere* 158 (2016) 131–142.
- [5] S. Eladak, T. Grisin, D. Moison, M.J. Guerin, T. N'Tumba-Byn, S. Pozzi-Gaudin, A. Benachi, G. Livera, V. Rouiller-Fabre, R. Habert, *Fertil. Steril.* 103 (2015) 0015–0282.
- [6] E. Yamazaki, N. Yamashita, S. Taniyasu, J. Lam, P.K.S. Lam, H. Moon, Y. Jeong, P. Kannan, H. Achyuthan, N. Munuswamy, K. Kannan, *Ecotoxicol. Environ. Safe* 122 (2015) 565–572.
- [7] B. Castro, P. Sánchez, J.M. Torres, E. Ortega, *Environ. Res.* 142 (2015) 281–287.
- [8] C. Liao, F. Liu, K. Kannan, *Environ. Sci. Technol.* 46 (2012) 6515–6522.
- [9] J.R. Rochester, A.L. Bolden, *Environ. Health Perspect.* 123 (2015) 643–650.
- [10] E. Danzl, K. Sei, S. Soda, M. Ike, M. Fujita, *Int. J. Environ. Res. Public Health* 6 (2009) 1472–1484.
- [11] N. Cabaton, C. Dumont, I. Severin, *Toxicology* 255 (2009) 15–24.
- [12] M. Audebert, L. Dolo, E. Perdu, J. Cravedi, D. Zalko, *Arch. Toxicol.* 85 (2011) 1463–1473.
- [13] M.Y. Chen, M. Ike, M. Fujita, *Environ. Toxicol.* 17 (2002) 80–86.
- [14] S. Kitamura, T. Suzuki, S. Seigo, R. Kohta, N. Jinno, K. Sugihara, S. Yoshihara, N. Fujimoto, H. Watanabe, H. Ohta, *Toxicol. Sci.* 84 (2005) 249–259.
- [15] N. Cabaton, M.C. Chagnon, J.C. Lhuguenot, J.P. Cravedi, D. Zalko, *J. Agric. Food Chem.* 54 (26) (2006) 10307–10314.
- [16] F. Pana, T. Xu, L. Yang, X. Jiang, L. Zhang, *Acta Part A: Mol. Biomol. Spectrosc.* 132 (2014) 795–802.
- [17] G. Liu, S. You, Y. Tan, N. Ren, *Environ. Sci. Technol.* 51 (2017) 2339–2346.
- [18] A. Tsitonaki, B. Petri, M. Crimi, H. Mosbaek, R.L. Siegrist, P.L. Bjerg, *Crit. Rev. Environ. Sci. Technol.* 40 (2010) 55–91.
- [19] P.R. Shukla, S.B. Wang, H.Q. Sun, H.M. Ang, M. Tade, *Appl. Catal. B* 100 (2010) 529–534.
- [20] G.P. Anipsitakis, D.D. Dionysiou, *Environ. Sci. Technol.* 37 (2003) 4790–4797.
- [21] Y. Feng, D. Wu, Y. Deng, T. Zhang, K. Shih, *Environ. Sci. Technol.* 50 (2016) 3119–3127.
- [22] R. Yuan, S.N. Ramjaun, Z. Wang, J. Liu, *J. Hazard. Mater.* 196 (2011) 173–179.
- [23] T. Zhang, Y. Chen, Y. Wang, J. Le Roux, Y. Yang, J. Croue, *Environ. Sci. Technol.* 48 (2014) 5868–5875.
- [24] H.V. Lutze, S. Bircher, I. Rapp, N. Kerlin, R. Bakkour, M. Geisler, C.V. Sonntag, T.C. Schmidt, *Environ. Sci. Technol.* 49 (2015) 1673–1680.
- [25] H. Lee, H. Lee, J. Jeong, J. Lee, N.B. Park, C. Lee, *Chem. Eng. J.* 266 (2015) 28–33.
- [26] R. Matta, S. Tlili, S. Chiron, S. Barbat, *Environ. Chem. Lett.* 9 (2011) 347–353.
- [27] C. Liang, H.W. Su, *Ind. Eng. Chem. Res.* 48 (2009) 5558–5562.
- [28] W.D. Oh, S.K. Lua, Z. Dong, T.T. Lim, J. Mater. Chem. A 2 (2014) 15836–15845.
- [29] P.D. Hu, M.C. Long, *Appl. Catal. B* 181 (2016) 103–117.
- [30] F. Ghanbari, M. Moradi, *J. Chem. Eng.* 310 (2017) 41–62.
- [31] P. Shi, R. Su, F. Wan, M. Zhu, D. Li, S. Xu, *Appl. Catal. B* 123–124 (2012) 265–272.
- [32] T. Zeng, X. Zhang, S. Wang, H. Niu, Y. Cai, *Environ. Sci. Technol.* 49 (2015) 2350–2357.
- [33] Y. Ji, D. Kong, J. Lu, H. Jin, F. Fang, X. Yin, Q. Zhou, *J. Hazard. Mater.* 313 (2016) 229–237.
- [34] D. Han, J. Wan, Y. Ma, Y. Wang, Y. Li, D. Li, Z. Guan, *Chem. Eng. J.* 269 (2015) 425–433.
- [35] Y. Leng, W. Guo, X. Shi, Y. Li, L. Xing, *Ind. Eng. Chem. Res.* 52 (2013) 13607–13612.
- [36] Y. Fan, W. Ma, J. He, Y. Du, *RSC Adv.* 7 (2017) 36193–36200.
- [37] X. Duan, H. Sun, J. Kang, Y. Wang, S. Indrawirawan, S. Wang, *ACS Catal.* 5 (2015) 4629–4636.
- [38] X. Duan, C. Sua, J. Miao, Y. Zhong, Z. Shao, S. Wang, H. Sun, *Appl. Catal. B: Environ.* 220 (2018) 626–634.
- [39] G.P. Anipsitakis, D.D. Dionysiou, *Environ. Sci. Technol.* 38 (2004) 3705–3712.
- [40] D.G. Barceloux, *Clin. Toxicol.* 37 (1999) 201–216.
- [41] P. Hu, M. Long, *Appl. Catal. B: Environ.* 181 (2016) 103–117.
- [42] G.P. Anipsitakis, E. Stathatos, D.D. Dionysiou, *J. Phys. Chem. B* 109 (2005) 13052–13055.
- [43] Y. Ren, L. Lin, J. Ma, J. Yang, J. Feng, Z. Fan, *Appl. Catal. B: Environ.* 165 (2015) 572–578.
- [44] Q. Yang, H. Choi, D.D. Dionysiou, *Appl. Catal. B: Environ.* 74 (2007) 170–178.
- [45] Q. Yang, H. Choi, Y. Chen, D.D. Dionysiou, *Appl. Catal. B: Environ.* 77 (2008) 300–307.
- [46] W. Zhang, H.L. Tay, S.S. Lim, Y. Wang, Z. Zhong, R. Xu, *Appl. Catal. B: Environ.* 95 (2010) 93–99.
- [47] P.H. Shi, R.J. Su, S.B. Zhu, M.C. Zhu, D.X. Li, S.H. Xu, *J. Hazard. Mater.* 229 (2012) 331–339.
- [48] X.Y. Chen, J.W. Chen, X.L. Qiao, D.G. Wang, X.Y. Cai, *Appl. Catal. B: Environ.* 80 (2008) 116–121.
- [49] K.H. Chan, W. Chu, *Water Res.* 43 (2009) 2513–2521.
- [50] Y. Feng, J.H. Liu, D.L. Wu, Z.Y. Zhou, Y. Deng, T. Zhang, K.M. Shih, *J. Chem. Eng.* 280 (2015) 514–524.
- [51] Q. Yang, H. Choi, S.R. Al-Abed, D.D. Dionysiou, *Appl. Catal. B* 88 (2009) 462–469.
- [52] T. Zhang, H.B. Zhu, J.P. Croue, *Environ. Sci. Technol.* 47 (2013) 2784–2791.
- [53] Y. Ding, L. Zhu, A. Huang, X. Zhao, X. Zhang, H. Tang, *Catal. Sci. Technol.* 2 (2012) 1977–1984.
- [54] S.H. Hameed, C. Karthikeyan, S. Sasikumar, V.S. Kumar, S. Kumaresan, G. Ravi, *J. Mater. Chem. B* 1 (2013) 5950–5962.
- [55] S.B. Hammouda, F. Zhao, Z. Safaei, I. Babu, D.L. Ramasamy, M. Sillanpää, *Appl. Catal. B: Environ.* 218 (2017) 119–136.
- [56] M.A. Pena, J.L.G. Fierro, *Chem. Rev.* 101 (2001) 1981–2017.
- [57] A. Grimaud, K.J. May, C.E. Carlton, Y.L. Lee, M. Risch, W.T. Hong, J.G. Zhou, Y. Shao-Horn, *Nat. Commun.* 4 (2013) 2439.
- [58] X.T. Pang, Y. Guo, Y.T. Zhang, B.B. Xu, F. Qi, *J. Chem. Eng.* 304 (2016) 897–907.
- [59] K.Y.A. Lin, Y.C. Chen, Y.F. Lin, *Chem. Eng. Sci.* 160 (2017) 96–105.
- [60] G. Ben, A. Desheng, M.A. Jingtao, D. Changsheng, L. Xuping, *J. Rare Earth* 29 (2011) 673–677.
- [61] J.L. Sotelo, G. Ovejero, F. Martinez, J.A. Melero, A. Milieni, *Appl. Catal. B: Environ.* 47 (2004) 281–294.
- [62] L. Zhang, Q. Zhou, Q. He, T. He, J. Power Sources 195 (2010) 6356–6366.
- [63] H. Seim, M. Nieminen, L. Niinistö, H. Fjellvåg, L.S. Johansson, *Appl. Surf. Sci.* 112 (1997) 243–250.
- [64] P. Kayser, J.A. Alonso, A. Munoz, M.T. Fernandez-Díaz, *Acta Mater.* 126 (2017) 114–123.

- [65] H. Falcon, J.A. Barbero, G. Araujo, M.T. Casais, M.J. Martinez-Lope, J.A. Alonso, J.L.G. Fierro, *Appl. Catal. B: Environ.* 53 (2004) 37–45.
- [66] R.R. Solís, F. Javier Rivas, O. Gimeno, *Appl. Catal. B: Environ.* (2017) 83–92.
- [67] Y. Tomioka, T. Okuda, Y. Okimoto, Y. Tokura, *Phys. Rev. B* 61 (2000) 422–427.
- [68] K.I. Kobayashi, T. Kimura, Y. Tomioka, Y. Tokura, *Phys. Rev. B* 59 (17) (1999) 69977–11162.
- [69] M. Siddiquea, S.K. Durranib, E. Ahmeda, J. Ceram. Process. Res. 16 (2015) 515–518.
- [70] B. Orayech, L.O.S. Martin, I.U. Olabarria, J.M. Igartua, *Dalton Trans.* 44 (2015) 13716–13734.
- [71] X. Chen, J. Chen, X. Qiao, D. Wang, X. Cai, *Appl. Catal. B: Environ.* 80 (2008) 116–121.
- [72] J. Li, Y. Yi, P. Shi, Q. Wang, D.X. Li, H. Asif, M. Yang, *Acta Phys.-Chim. Sin.* 30 (2014) 1720–1726.
- [73] P. Hu, M. Long, *Appl. Catal. B: Environ.* 181 (2016) 103–117.
- [74] R.R. Solís, F.J. Rivas, Olga Gimeno, *Appl. Catal. B* 200 (2017) 83–92.
- [75] H. Gong, W. Chu, S.H. Lam, A.Y. Lin, *Chemosphere* 167 (2017) 415–421.
- [76] Y.R. Wang, W. Chu, *J. Hazard. Mater.* 186 (2011) 1455–1461.
- [77] W.D. OH, Z. Dong, T.T. Lim, *Appl. Catal. B: Environ.* 194 (2016) 169–201.
- [78] D.G. Driscoll, J. Carter, M. Janet, J. Williamson, E.E. Joyce, L.D. Putnam, *Hydrology of the Black Hills Area, South Dakota, Water Resources Investigation Report 02-4094*. USDI, US Geological Survey, (2002) 150 pp..
- [79] A. Al-Anazi, W.H. Abdelraheem, C. Han, M.N. Nadagouda, L. Sygello, M.K. Arfanis, P. Falras, V.K. Sharma, D.D. Dionysiou, *Appl. Catal. B* (2018), <http://dx.doi.org/10.1016/j.apcatb.2017.08.054>.
- [80] Q. Zhua, S. Maenoa, M. Sasaki, T. Miyamotoa, M. Fukushimaa, *Appl. Catal. B: Environ.* 163 (2015) 459–466.
- [81] M. Pagano, A. Volpe, G. Mascolo, A. Lopez, V. Locaputo, R. Ciannarella, *Chemosphere* 86 (2012) 329–334.
- [82] P. Shukla, S. Wang, K. Singh, H.M. Ang, M.O. Tade, *Appl. Catal. B: Environ.* 99 (2010) 163–169.
- [83] G. McLachlan, J. Muller, S. Rokita, C. Burrows, *Inorg. Chim. Acta* 251 (1996) 193–199.
- [84] W. Chu, C.Y. Kwan, K.H. Chan, S.K. Kam, *J. Hazard. Mater.* 121 (2005) 119–126.
- [85] G.P. Anipsitakis, D.D. Dionysiou, M.A. Gonzalez, *Environ. Sci. Technol.* 40 (2006) 1000–1007.
- [86] G.V. Buxton, C.L. Greenstock, W.P. Helman, A.B. Ross, *J. Phys. Chem. Ref. Data* 17 (1988) 513–886.
- [87] C.L. Clifton, R.E. Huie, *Int. J. Chem. Kinet.* 21 (1989) 677–687.
- [88] R. Jameton, J. Muller, C. Burrows, *C. R. Chim.* 5 (2002) 461–466.
- [89] K.-A. Lin, Y.C. Chen, C.-F. Huang, *Sep. Purif. Technol.* 170 (2016) 173–182.
- [90] Y. Qian, X. Zhou, Y. Zhang, P. Sun, W. Zhang, J. Chen, X. Guo, X. Zhang, *J. Chem. Eng.* 279 (2015) 538–546.
- [91] J. Sharma, I.M. Mishra, D.D. Dionysiou, V. Kumar, *Chem. Eng. J.* 276 (2015) 193–204.
- [92] J.A. Khan, X. He, H.M. Khan, N.S. Shah, D.D. Dionysiou, *Chem. Eng. J.* 318 (2013) 376–383.
- [93] G.V. Buxton, C.L. Greenstock, W.P. Helman, A.B. Ross, *J. Phys. Chem. Ref. Data* 17 (1988) 513–886.
- [94] S. Khan, X. He, J.A. Khan, H.M. Khan, D.L. Boccelli, D.D. Dionysiou, *Chem. Eng. J.* 318 (2017) 135–142.
- [95] B. Gao, Z. Safaei, I. Babu, S. Iftekhara, E. Lakovleva, V. Srivastava, B. Doshi, S.B. Hammouda, S. Kalliola, Mika Sillanpää, *J. Photochem. Photobiol. A: Chem.* 348 (2017) 150–160.